

Statistical mechanics of triangulated ribbons

Boris Mergell,* Mohammad R. Ejtehadi, and Ralf Everaers
Max-Planck-Institut für Polymerforschung, Postfach 3148, D-55021 Mainz, Germany

(Dated: November 2, 2018)

We use computer simulations and scaling arguments to investigate statistical and structural properties of a semiflexible ribbon composed of isosceles triangles. We study two different models, one where the bending energy is calculated from the angles between the normal vectors of adjacent triangles, the second where the edges are viewed as semiflexible polymers so that the bending energy is related to the angles between the tangent vectors of next-nearest neighbor triangles. The first model can be solved exactly whereas the second is more involved. It was recently introduced by Liverpool and Golestanian Phys.Rev.Lett. **80**, 405 (1998), Phys.Rev.E **62**, 5488 (2000) as a model for double-stranded biopolymers such as DNA. Comparing observables such as the autocorrelation functions of the tangent vectors and the bond-director field, the probability distribution functions of the end-to-end distance, and the mean squared twist we confirm the existence of local twist correlation, but find no indications for other predicted features such as twist-stretch coupling, kinks, or oscillations in the autocorrelation function of the bond-director field.

PACS numbers: 87.15.Aa,87.15.La,61.41.+e

I. INTRODUCTION

A characteristic feature of many biopolymers is their high bending stiffness. Contour lengths of the order of μm and persistence lengths of the order of $50 nm$ in the case of DNA even allow microscopy techniques to be used to directly observe their structure and dynamics [3, 4]. The model mostly used to interpret recent experimental data of micromechanical manipulations of single DNA chains [3, 4, 5, 6, 7, 8] is that of the Kratky-Porod wormlike chain in which the polymer flexibility is determined by a single length, the persistence length l_p . Generalizations account for the chain helicity and coupling terms between bending, stretching, and twisting allowed by symmetry [9, 10, 11, 12, 13, 14, 15, 16, 17, 18, 19, 20]. All these continuum models of DNA neglect the double-stranded structure of DNA and one may ask, if this feature could not cause qualitative different behavior.

The bending stiffness of single- and double-stranded DNA, for example, differs by a factor of 25 [21]. The simplest model which takes the double-strandedness into account is the railway-track model [22] where two wormlike chains are coupled with harmonic springs. In two dimensions one finds drastical consequences: the bending fluctuations in the plane of the ribbon are strongly suppressed. The molecule becomes effectively stiffer on larger length scales. But the relevant question is: what are the effects in three dimensions? Liverpool *et al* [1, 2] investigated a version of the railway-track model in three dimensions where bending in the plane of the ribbon is forbidden by a constraint. Using analytical and simulation techniques they predict the existence of a low temperature regime where ribbons adopt a kink-rod structure due to a spontaneously appearing short-range twist

structure resulting in an oscillatory behavior of the autocorrelation function of the bond-director field. Furthermore a twist-stretch coupling is predicted.

We study the discretized version of the simulation model of Liverpool *et al* [1, 2] in the low temperature regime with the help of scaling arguments and MC simulations. In order to understand and to quantify the effects arising from the local twist structure of the Liverpool model we compare it with an analytically more tractable model where the bending stiffness is defined via the interaction of the normal vectors so that there is no tendency to helical structures. Furthermore, we perform several MC simulation runs with an additional external force in order to test if the preferred buckling mechanism occurs via kinks.

II. CONTINUOUS DESCRIPTION OF TWO COUPLED SEMIFLEXIBLE CHAINS

A ribbon is an inextensible, unsharable rod which can be parameterized by the arclength s . To each point s one attaches a triad of unit vectors $\{\mathbf{d}_i(s)\}$. The vectors $\mathbf{d}_1(s)$ and $\mathbf{d}_2(s)$ are directed along the two principle axis of the cross section, the vector $\mathbf{d}_3(s)$ is the tangent vector. As the triad is an orthonormal basis set they satisfy kinematic equations of the form

$$\frac{d}{ds}\mathbf{d}_i(s) = \epsilon_{ijk}u_j(s)\mathbf{d}_k(s) \quad (1)$$

with ϵ_{ijk} being the alternating tensor and $u_j(s)$ representing bend ($u_1(s)$) out-of-plane, and $u_2(s)$ in-plane) and twist strains ($u_3(s)$) respectively. One can find a relation between the ordinary Frenet equations containing only

*Electronic address: mergell@mpip-mainz.mpg.de

two parameters, the curvature $\kappa(s)$ and the torsion $\tau(s)$

$$\frac{d\mathbf{t}(s)}{ds} = \kappa(s)\mathbf{n}(s) \quad (2)$$

$$\frac{d\mathbf{b}(s)}{ds} = -\tau(s)\mathbf{n}(s) \quad (3)$$

$$\frac{d\mathbf{n}(s)}{ds} = \tau(s)\mathbf{b}(s) - \kappa(s)\mathbf{t}(s) \quad (4)$$

and Eqs. (1) by fixing $\mathbf{d}_3(s) = \mathbf{t}(s)$ so that $\mathbf{d}_1(s)$ and $\mathbf{d}_2(s)$ are given by a rotation around $\mathbf{t}(s)$ with angle $\Psi(s)$. In this context $\Psi(s)$ can be seen as the twist angle [17, 23]. A straightforward calculation gives for the generalized torsions: $u_1(s) = -\frac{d}{ds}\mathbf{d}_3(s) \cdot \mathbf{d}_2(s) = \kappa(s) \cos \Psi(s)$, $u_2(s) = \frac{d}{ds}\mathbf{d}_3(s) \cdot \mathbf{d}_1(s) = \kappa(s) \sin \Psi(s)$, and $u_3(s) = \frac{d}{ds}\mathbf{d}_1(s) \cdot \mathbf{d}_2(s) = \tau(s) + \frac{d\Psi(s)}{ds}$. The total Twist Tw of a ribbon is thus given by the integration of the local twist $u_3(s)$ along the contour normalized by the factor 2π

$$Tw = \frac{1}{2\pi} \int_0^L u_3(s) ds \quad (5)$$

with L being the contour length. Together with the parameter set $\hat{u}_i(s)$, which determines whether the stress-free reference configuration includes spontaneous curvature and twist, the elastic part of the Hamiltonian is usually defined by quadratic terms in $u_i(s) - \hat{u}_i(s)$ [11, 12, 13, 14, 15, 16, 17, 18, 19, 20, 24].

It is an interesting question to which extent this generic description applies to more microscopic models of DNA [25]. The simplest case is that of a ‘‘railway track’’ or ladder model consisting of two (or more) semiflexible chains

$$\mathcal{H}_{tt} = \frac{k}{2} \int_0^L ds \left\{ \left(\frac{d^2\mathbf{r}_1(s)}{ds^2} \right)^2 + \left(\frac{d^2\mathbf{r}_2(s)}{ds^2} \right)^2 \right\}, \quad (6)$$

plus a coupling between opposite points on different chains [22]. Liverpool *et al* [1, 2] considered the limit where the distance a between the coupling points (i.e. the width of the ribbon) is imposed as a rigid constraint which prevents bending in the plane of the ribbon: $\frac{d\mathbf{t}(s)}{ds} \cdot \mathbf{b}(s) = 0$ where $\mathbf{t}(s) = \frac{d\mathbf{r}(s)}{ds}$ is the tangent vector to the mid-curve $\mathbf{r}(s) = \mathbf{r}_1(s) - \frac{a}{2} = \mathbf{r}_2(s) + \frac{a}{2}$ and $\mathbf{b}(s)$ is the bond-director pointing from one strand to the other. Note, that the constraint is equivalent to $\Psi(s) = 0$. Rewriting Eq. (6) in terms of ribbon variables they found

$$\mathcal{H}_{tt} = \frac{k}{2} \int_0^L ds \left\{ 2 \left(\frac{d^2\mathbf{r}(s)}{ds^2} \right)^2 + \frac{a^2}{2} \left(\frac{d^2\mathbf{b}(s)}{ds^2} \right)^2 \right\} \quad (7)$$

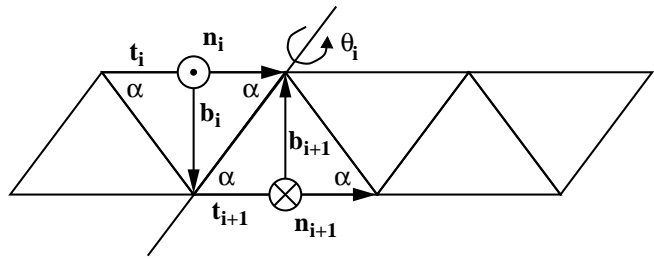


FIG. 1: Illustration of the used variables. The length of each triangle $|\mathbf{t}_i|$ corresponds to the bond length b and the height $|\mathbf{b}_i| = \frac{1}{2}b \tan(\alpha)$ defines the strand separation length. $\{\theta_i\}$ term the folding angles.

which can also be expressed as

$$\left(\frac{d\mathbf{t}}{ds} \right)^2 = \kappa^2 \quad (8)$$

$$\begin{aligned} \left(\frac{d^2\mathbf{b}}{ds^2} \right)^2 &= \left(\frac{du_1}{ds} \right)^2 + (u_1^2 - u_3^2)^2 + \left(\frac{du_3}{ds} \right)^2 \\ &= \left(\frac{d\kappa}{ds} \right)^2 + \left(\frac{d\tau}{ds} \right)^2 + (\kappa^2 - \tau^2)^2. \end{aligned} \quad (9)$$

Note, that henceforth we use $\mathbf{b}(s)$ as the bond-director and $\mathbf{n}(s)$ as the normal vector to the ribbon plane.

III. GEOMETRY OF TRIANGULATED RIBBONS

Following Liverpool *et al* [1, 2] we consider ribbons discretized by triangulation. In order to extract some fundamental properties of double-stranded semiflexible polymers we consider a ribbon-like system composed of isosceles triangles as shown in Fig. 1. The orientation of each triangle is given by $N - 1$ rotations around the edges of the triangles with folding angles $\{\theta_i\}$. N is the number of triangles characterized by a set of trihedrons $\{\mathbf{t}_i, \mathbf{b}_i, \mathbf{n}_i\}$ where \mathbf{t}_i is the tangent vector of the i th triangle, \mathbf{b}_i is the bond-director, and \mathbf{n}_i is the normal vector. Going from one set of trihedrons $\{\mathbf{t}_i, \mathbf{b}_i, \mathbf{n}_i\}$ to the neighbor set $\{\mathbf{t}_{i+1}, \mathbf{b}_{i+1}, \mathbf{n}_{i+1}\}$ implies a rotation \mathcal{R}_i around the edge between the respective triangles with angle θ_i and a reflection of \mathbf{b}_i and \mathbf{n}_i , i.e.

$$\begin{pmatrix} \mathbf{t}_{i+1} \\ \mathbf{b}_{i+1} \\ \mathbf{n}_{i+1} \end{pmatrix} = \mathcal{T}\mathcal{R}_i \begin{pmatrix} \mathbf{t}_i \\ \mathbf{b}_i \\ \mathbf{n}_i \end{pmatrix} \quad (10)$$

with

$$\mathcal{T} = \begin{pmatrix} 1 & 0 & 0 \\ 0 & -1 & 0 \\ 0 & 0 & -1 \end{pmatrix} \quad (11)$$

$$\mathcal{R}_i = \begin{pmatrix} \mathbf{t}_i \cdot \mathbf{t}_{i+1} & \mathbf{t}_i \cdot \mathbf{b}_{i+1} & \mathbf{t}_i \cdot \mathbf{n}_{i+1} \\ \mathbf{b}_i \cdot \mathbf{t}_{i+1} & \mathbf{b}_i \cdot \mathbf{b}_{i+1} & \mathbf{b}_i \cdot \mathbf{n}_{i+1} \\ \mathbf{n}_i \cdot \mathbf{t}_{i+1} & \mathbf{n}_i \cdot \mathbf{b}_{i+1} & \mathbf{n}_i \cdot \mathbf{n}_{i+1} \end{pmatrix}. \quad (12)$$

The matrix product \mathcal{TR}_i can be viewed as a transfer matrix. The evaluation of the scalar products of \mathcal{R}_i gives

$$\begin{aligned}
\mathcal{R}_{i,11} &= \cos(\theta_i) + \cos(\alpha)^2 (1 - \cos(\theta_i)) \\
\mathcal{R}_{i,12} &= -\cos(\alpha) \sin(\alpha) (1 - \cos(\theta_i)) \\
\mathcal{R}_{i,13} &= -\sin(\alpha) \sin(\theta_i) \\
\mathcal{R}_{i,21} &= \cos(\alpha) \sin(\alpha) (1 - \cos(\theta_i)) \\
\mathcal{R}_{i,22} &= \cos(\theta_i) + \sin(\alpha)^2 (1 - \cos(\theta_i)) \\
\mathcal{R}_{i,23} &= -\cos(\alpha) \sin(\theta_i) \\
\mathcal{R}_{i,31} &= \sin(\alpha) \sin(\theta_i) \\
\mathcal{R}_{i,32} &= \cos(\alpha) \sin(\theta_i) \\
\mathcal{R}_{i,33} &= \cos(\theta_i).
\end{aligned} \tag{13}$$

In order to quantify properties such as bending and twisting within the given discretization we study the relation between the folding angles θ_i and these quantities which is illustrated in Fig. 2. One recognizes that the chain is not bent in case of $\theta_i - \theta_{i+1} = \delta\theta_i = 0$ and that one gains purely twisted structures if $\theta_i \equiv \text{const}$. On the other hand the chain is untwisted but bent if $\delta\theta_i = 2\theta_i$. In case of $\theta_i \neq \pm\theta_{i+1}$ and $\theta_i \neq 0$ the chain is bent and twisted simultaneously resulting in solenoidal/torsional structures as is illustrated in Fig. 2(f). A kink is characterized by unlike twists meeting at an edge as it is shown in Fig. 2(d).

Due to the triangulation of the ribbon one has to consider three triangles to calculate the discretized expressions for the out-of-plane bending strain $u_1(s) = -\frac{d}{ds} \mathbf{t}(s) \cdot \mathbf{n}(s) \approx -\frac{\mathbf{t}(s+\Delta s) - \mathbf{t}(s)}{\Delta s} \cdot \mathbf{n}(s) = -\frac{1}{\Delta s} \mathbf{t}(s+\Delta s) \cdot \mathbf{n}(s)$ and the twist strain $u_3(s) = \frac{d}{ds} \mathbf{b}(s) \cdot \mathbf{n}(s) \approx \frac{\mathbf{b}(s+\Delta s) - \mathbf{b}(s)}{\Delta s} \cdot \mathbf{n}(s) = \frac{1}{\Delta s} \mathbf{b}(s+\Delta s) \cdot \mathbf{n}(s)$ which we call κ_i and τ_i respectively. The local curvature κ_i and the local twist rate τ_i between triangle i and $i+2$ are therefore given by

$$\kappa_i \equiv -\frac{1}{b} \sum_{j=i}^{i+1} \mathbf{n}_j \cdot \mathbf{t}_{j+1} \approx \frac{\sin(\alpha)}{b} \delta\theta_i \tag{14}$$

$$\tau_i \equiv \frac{1}{b} \sum_{j=i}^{i+1} \mathbf{n}_j \cdot \mathbf{b}_{j+1} \approx \frac{\cos(\alpha)}{b} (\theta_i + \theta_{i+1}), \tag{15}$$

where the accuracy of the right-hand side expressions only depends on the refinement of the discretization, i.e. on the values of b and α . Hence a spontaneous bending can be introduced via an additional term to the Hamiltonian with $\mathcal{H}_{curv} = k_{curv} \sum_i \left(\sum_{j=i}^{i+1} \mathbf{n}_j \cdot \mathbf{t}_{j+1} - \delta\theta_{sp,i} \right)^2$ and a spontaneous twist can be introduced by an additional term $\mathcal{H}_{Tw} = k_{Tw} \sum_i \left(\sum_{j=i}^{i+1} \mathbf{n}_j \cdot \mathbf{b}_{j+1} - \theta_{sp,i} \right)^2$. Note, that the total twist Tw is given by $Tw = 1/(2\pi) \sum_i \tau_i$.

IV. MODEL DESCRIPTION

The bending stiffness within the given discretization can be taken into account by various interactions. One

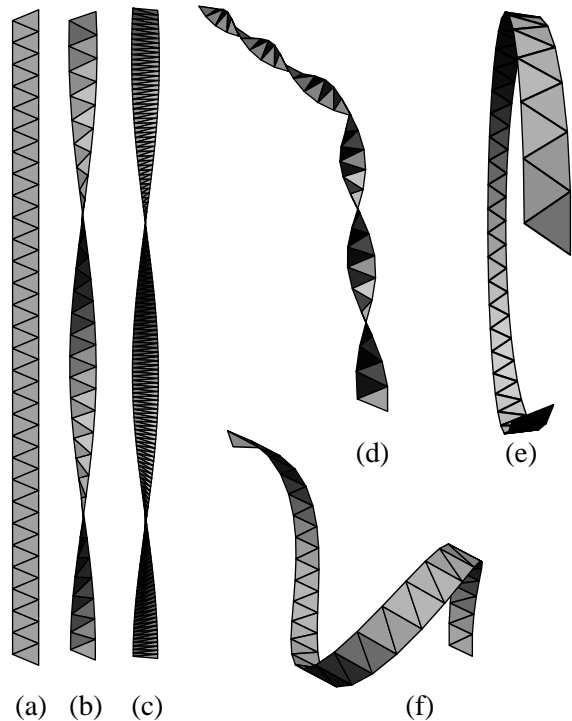


FIG. 2: Illustration of bending, twisting, and kinking. (a) A flat ribbon as ground state conformation. (b) A twisted structure (c) The same twisted structure obtained with a smoother discretization. (d) Unlike twists meeting at the center resulting in a kink with θ_i positive for $i < N/2$, negative for $i \geq N/2$, and $|\theta_i| = |\theta_{i+1}|$, i.e. $\delta\theta_i = 0, \forall i \neq N/2$ and $\delta\theta_{N/2} = 2\theta_{N/2}$. (e) A bent structure. (f) A mixture of bent and twist resembling a solenoidal structure.

possible definition of a bending stiffness, which makes the problem analytically tractable, is a nearest neighbor interaction (plaquette stiffness) between the normal vectors $\{\mathbf{n}_i\}$ in analogy to the triangulation of vesicles [26] which results in the following Hamiltonian

$$\frac{\mathcal{H}_{nn}}{k_B T} = k \sum_{i=1}^{N-1} (1 + \mathbf{n}_i \cdot \mathbf{n}_{i+1}). \tag{16}$$

In contrast Liverpool *et al* [1, 2] were interested in the statistical mechanics of coupled wormlike chains and therefore chose a next-nearest neighbor interaction (edge stiffness) between the tangent vectors $\{\mathbf{t}_i\}$ with rigidity k so that the Hamiltonian is given by

$$\frac{\mathcal{H}_{tt}}{k_B T} = k \sum_{i=1}^{N-2} (1 - \mathbf{t}_i \cdot \mathbf{t}_{i+2}). \tag{17}$$

Both definitions lead to a flat ribbon as the ground state conformation for zero temperatures $T = 0$.

The above defined interactions lead to very distinct conformational features of the ribbon which can be understood by building up the ribbon just by adding successively the triangles in the absence of thermal fluctuations. Assuming that $\theta_1 \neq 0$ all subsequent angles θ_i with $i > 1$ vanish in the case of the nearest neighbor interaction (\mathcal{H}_{nn}). In contrast the tangent-tangent interaction (\mathcal{H}_{tt}) leads to the formation of a helix with $\theta_i = \theta_{i+1}$ as a result of the enforced alignment of the tangent vectors. This suggests a correlation of the folding angles $\{\theta_i\}$ which entails at least locally helical structures.

Assuming that the chains are rather stiff (continuum limit), i.e. small folding angles θ_i , one can expand the Hamiltonians with regard to θ_i . Since \mathcal{H}_{nn} is diagonal in θ_i , it is sufficient to consider terms up to second order. \mathcal{H}_{tt} contains coupling terms between θ_i and θ_{i+1} which makes it necessary to keep terms up to fourth order in the analysis:

$$\begin{aligned} \frac{\mathcal{H}_{nn}}{k_B T} &\approx \frac{k}{2} \sum_{i=1}^{N-1} \theta_i^2 & (18) \\ \frac{\mathcal{H}_{tt}}{k_B T} &\approx \frac{k}{2} \sum_{i=1}^{N-2} \left\{ \sin(\alpha)^2 \delta\theta_i^2 \left(1 - \frac{1}{12} \delta\theta_i^2 \right) \right. \\ &\quad \left. + \sin(\alpha)^2 \cos(\alpha)^2 \theta_i^2 \theta_{i+1}^2 \right\} & (19) \end{aligned}$$

with $\delta\theta_i = \theta_i - \theta_{i+1}$.

V. MC SIMULATION

Both models have local interactions and can be studied conveniently using a dynamic MC scheme. Trial moves consist of small random changes of the folding angles by a small amplitude $1/\sqrt{k}$, where k is the bending stiffness, and are accepted or rejected according to the Metropolis scheme [27]. In the simulations we always use the full Hamiltonians Eq. (16) and (17). MC moves changing the folding angles correspond to the well-known Pivot algorithm [28]. The conformations are subsequently recalculated from Eqs. (10)-(13) and analyzed. Each simulation run comprises 100000 MC-moves where one MC move corresponds to $N - 1$ trials with N being the number of triangles. The longest correlation time we observed was of the order of 50 MC moves for the total twist of the chain. In order to check if equilibrium is reached we compared simulation runs with a flat initial conformation, i.e. $\theta_i = 0$, with simulation runs with crumpled conformations corresponding to equally distributed angles θ_i out of the interval $[-1/\sqrt{k}; 1/\sqrt{k}]$. Both runs yield the same results for the calculated observables.

VI. PLAQUETTE STIFFNESS

Since the Hamiltonian \mathcal{H}_{nn} of Eq. (18) is quadratic and diagonal in θ_i the solution in angle space is trivial. As a consequence of the independence of successive folding angles it yields $\langle \theta_i \theta_j \rangle = \frac{1}{k} \delta_{ij}$ and $\langle \mathcal{A} \rangle = \langle \prod_{k=i}^j (\mathcal{TR}_k) \rangle = \langle \mathcal{TR}_k \rangle^{j-i}$ where the matrix product is carried out in the eigenvector basis of $\langle \mathcal{TR}_k \rangle$ (the eigenvectors depend only on the geometry of the triangles). The diagonal elements of $\langle \mathcal{A} \rangle$ are the correlation functions $\langle \mathbf{t}_i \cdot \mathbf{t}_j \rangle, \langle \mathbf{b}_i \cdot \mathbf{b}_j \rangle, \langle \mathbf{n}_i \cdot \mathbf{n}_j \rangle$. Thus one calculates $\langle \mathcal{TR}_k \rangle$, diagonalizes it, raises it to the power of $j - i$, transforms it back, and performs the continuum chain limit with $s = (j - i)b$, $l_p = bk/\sin(\alpha)^2$, $a = \frac{1}{2}b \tan(\alpha)$, $(j - i) \rightarrow \infty$, $b \rightarrow 0$, i.e. $a \rightarrow 0$, where l_p is the persistence length, a is the strand separation, b is the Kuhn segment length, $0 < s < L$ is the arclength, and L is the contour length. Note that within this model α is a fixed parameter that determines bending characteristics of the ribbon. An exact expression for the autocorrelation functions is obtained:

$$\langle \mathbf{t}(0) \cdot \mathbf{t}(s) \rangle = \exp\left(-\frac{s}{l_p}\right) \quad (20)$$

$$\langle \mathbf{b}(0) \cdot \mathbf{b}(s) \rangle = \exp\left(-\frac{s}{l_p \tan(\alpha)^2}\right) \quad (21)$$

$$\langle \mathbf{n}(0) \cdot \mathbf{n}(s) \rangle = \exp\left(-\frac{s}{l_p \sin(\alpha)^2}\right). \quad (22)$$

For $\alpha = \pi/2$ one recovers the usual wormlike chain result for two dimensions. All crosscorrelation functions (the off-diagonal elements of $\langle \mathcal{A} \rangle$) vanish. Eqs. (21), (22) represent the persistence length $l_{p,in} = l_p \tan(\alpha)^2$ for bending within the plane of the ribbon and the persistence length $l_{p,out} = l_p \sin(\alpha)^2$ for bending out of the plane of the ribbon respectively [24]. This model was recently treated as a twisted zig-zag fiber within the framework of a two-angle model for studying structural properties of chromatin [29].

From the tangent-tangent correlation function one can calculate the mean squared end-to-end distance:

$$\begin{aligned} R_E^2 &= \langle (\mathbf{R}(L) - \mathbf{R}(0))^2 \rangle = \int_0^L ds_1 \int_0^L ds_2 \langle \mathbf{t}(s_1) \cdot \mathbf{t}(s_2) \rangle \\ &= 2Ll_p - 2l_p^2 \left(1 - \exp\left(-\frac{L}{l_p}\right) \right). \end{aligned} \quad (23)$$

Eqs. (20) and (23) are identical to results for single wormlike chains [30]. Eq. (23) interpolates between the limiting behaviors of random coils ($2Ll_p$) for $L \gg l_p$ and rigid rods (L^2) for $L \ll l_p$.

VII. EDGE STIFFNESS

In the following we present a simple scaling argument which allows us to rationalize the behavior of the Liver-

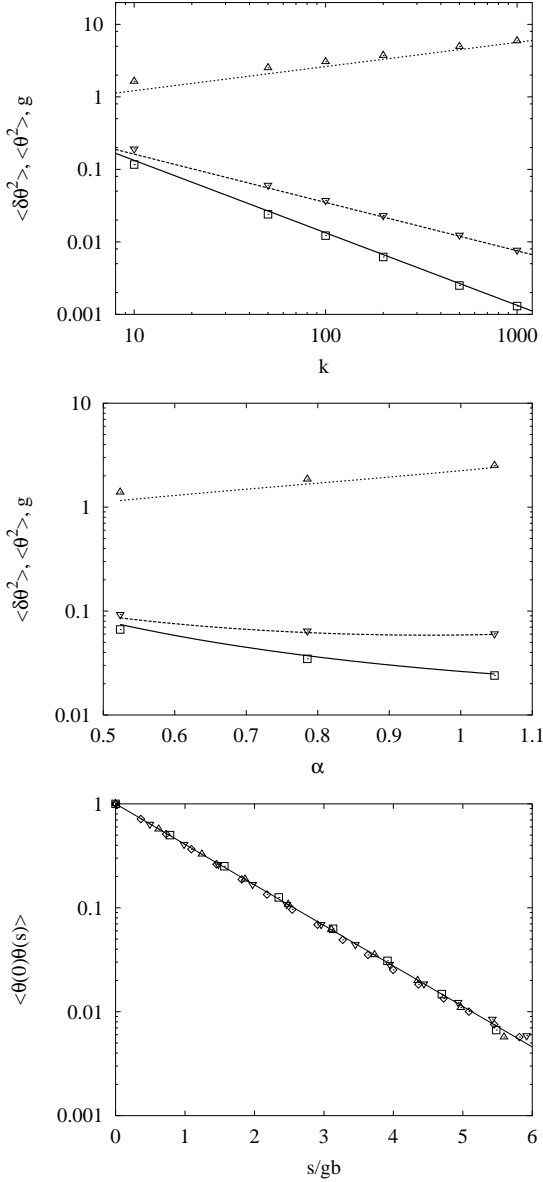


FIG. 3: (a), (b) Scaling plots for $\langle \theta_i^2 \rangle$ (downward triangles), $\langle \delta\theta_i^2 \rangle$ (squares), and g with $\alpha = \pi/3$ (upward triangles) and $k = 50$ respectively. (c) Numerical evidence for the derived expression of $\langle \theta_i \theta_j \rangle$. The data refer to $k = 50$ (squares), $k = 100$ (circles), $k = 200$ (upward triangles), $k = 500$ (downward triangles) and $\alpha = \pi/4$. We determine the correct prefactor $g_{fit} = 0.56 \pm 0.05$ of g from the numerical data of the folding angle correlation function $\langle \theta_i \theta_j \rangle$ which is our solely free parameter and use it for all following comparisons between scaling analysis and numerical results.

pool model. Consider first the $\delta\theta$ part of Eq. (19). In the absence of other terms the folding angles would perform a simple random walk with step length $\langle \delta\theta_i^2 \rangle = \frac{1}{k \sin(\alpha)^2}$. The leading term limiting the fluctuations of the folding angles around zero is of order $\mathcal{O}(\theta_i^4)$. The behavior of the coupled system can be inferred from scaling ar-

guments similar to those used for polymer adsorption. Consider a vanishing folding angle and follow the chain in either direction. Up to a characteristic number of steps g the folding angles will show simple diffusion. As a consequence the mean-squared folding angle averaged over this short segment is $\langle \theta_i^2 \rangle = g \langle \delta\theta_i^2 \rangle$ corresponding to a potential energy $\frac{E_{ex}}{k_B T} \sim g \langle \theta_i^4 \rangle \sim 3g \langle \theta_i^2 \rangle^2 \sim 3g^3 \langle \delta\theta_i^2 \rangle$. The free diffusion of the folding angles has to stop when this potential energy is of order $k_B T$, suggesting

$$\langle \delta\theta_i^2 \rangle = \frac{1}{k \sin(\alpha)^2} \quad (24)$$

$$g \sim \left(\frac{k \tan(\alpha)^2}{3} \right)^{\frac{1}{3}} \quad (25)$$

$$\langle \theta_i^2 \rangle = g \langle \delta\theta_i^2 \rangle \quad (26)$$

$$\frac{\langle \theta_i \theta_j \rangle}{\langle \theta_i^2 \rangle} = \exp\left(-\frac{|j-i|}{2g}\right). \quad (27)$$

Fig. 3 shows that these arguments are fully supported by the results of our MC simulations with $g = (0.56 \pm 0.05) \left(\frac{k \tan(\alpha)^2}{3} \right)^{\frac{1}{3}}$.

Using again the transfer matrix ansatz one obtains in the low temperature limit by considering only terms of the order $\mathcal{O}(\theta_i^2)$ the following expression for $\mathbf{t}_i \cdot \mathbf{t}_j$, $\mathbf{b}_i \cdot \mathbf{b}_j$ and $\mathbf{n}_i \cdot \mathbf{n}_j$:

$$\mathbf{t}_i \cdot \mathbf{t}_j = 1 - \frac{\sin(\alpha)^2}{2} \left(\sum_{k=i/2}^{j/2} \delta\theta_{2k} \right)^2 \quad (28)$$

$$\mathbf{b}_i \cdot \mathbf{b}_j = 1 - \frac{\cos(\alpha)^2}{2} \left(\sum_{k=i}^{j-1} \theta_k^2 + 2 \sum_{k=i}^{j-1} \sum_{k'=k+1}^{j-1} \theta_k \theta_{k'} \right) \quad (29)$$

$$\mathbf{n}_i \cdot \mathbf{n}_j = 1 - \frac{1}{2} \sum_{k=i/2}^{j/2} \delta\theta_{2k}^2 + \cos(\alpha)^2 \sum_{k=i}^{j-1} \sum_{k'=k+1}^{j-1} \theta_k \theta_{k'} \quad (30)$$

Note that i, j are either odd or even depending on which strand is under consideration. Without loss of generality we choose i, j to be even. First of all we use that $\langle \mathbf{t}(0) \cdot \mathbf{t}(s) \rangle$ has to interpolate between 1 for $s = 0$ and 0 for $s \rightarrow \infty$ and that the right hand side of Eq. (28) is the Taylor expansion up to first order of the exponential function $\exp\left(\frac{\sin(\alpha)^2}{2} \left(\sum_{k=i/2}^{j/2} \delta\theta_{2k} \right)^2\right)$. Substituting then $s = 2|j-i|b$ and $l_p = 4bk$, performing the continuum chain limit with $b \rightarrow 0$ and $\alpha \rightarrow \pi/2$ respectively, i.e. keeping the strand separation a constant, yields the following expression for the autocorrelation function of the tangent vectors:

$$\langle \mathbf{t}(0) \cdot \mathbf{t}(s) \rangle = \exp\left(-\frac{s}{l_p}\right). \quad (31)$$

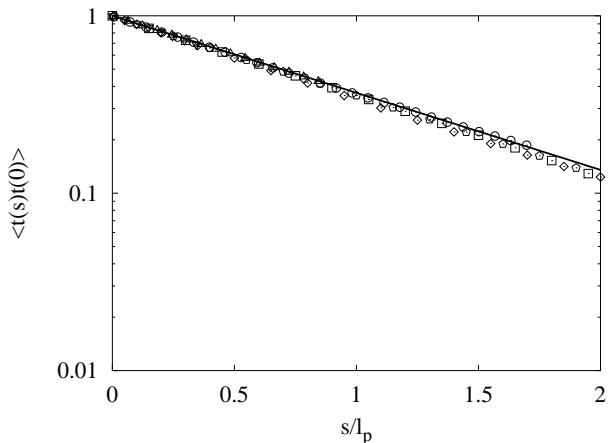


FIG. 4: Comparison of MC-data and analytical results (solid line) for the autocorrelation function of the tangent vectors with $k = 50$ (squares), $k = 100$ (circles), $k = 200$ (upward triangles), $k = 500$ (downward triangles) and $\alpha = \pi/3$, and $k = 50$ and $\alpha = \pi/4$ (diamonds), $\alpha = \pi/6$ (pentagons).

Thus the mean squared end-to-end distance R_E^2 becomes identical to Eq. (23). Eq. (31) is confirmed by our MC simulation data shown in Fig. 4.

To get an idea of the structural properties characterized by the autocorrelation function of the bond-directors $\langle \mathbf{b}_i \cdot \mathbf{b}_j \rangle$ we calculate the mean squared twist $\langle Tw(i, j)^2 \rangle$ of the ribbon. Following the definition of the local twist rate τ_i of Eq. (15) the total twist between two triangles of index i and j is just the sum of the local twist angles determined by the projections of the normal vector of the i th triangle onto the bond-director of the $(i + 1)$ th triangle, that is

$$Tw(i, j) = \frac{1}{2\pi} \sum_{k=i}^{j-1} \mathbf{n}_i \cdot \mathbf{b}_{i+1} = \frac{\cos(\alpha)}{2\pi} \sum_{k=i}^{j-1} \theta_k. \quad (32)$$

Comparing Eq. (29) and (32) we find for small twist angles

$$\langle \mathbf{b}_i \cdot \mathbf{b}_j \rangle = 1 - 2\pi^2 \langle Tw(i, j)^2 \rangle. \quad (33)$$

Hence the autocorrelation function of the bond-directors can be seen as a measure for the local twist structure of the ribbon.

In contrast to the plaquette stiffness model the angles θ_i are correlated (see Eq. (27)). Therefore the double summation over $\langle \theta_i \theta_j \rangle$ in Eq. (29) yields an analogous result as it is obtained in the calculation of the mean squared end-to-end distance of the wormlike chain model. Using the derived scaling expressions of Eqs. (25) and (26), the same substitutions as in Eq. (31), and performing the continuum chain limit one obtains the following relationship for the autocorrelation function of the bond-directors:

$$\langle \mathbf{b}(0) \cdot \mathbf{b}(s) \rangle = \exp(-2\pi^2 \langle Tw(0, s)^2 \rangle) \quad (34)$$

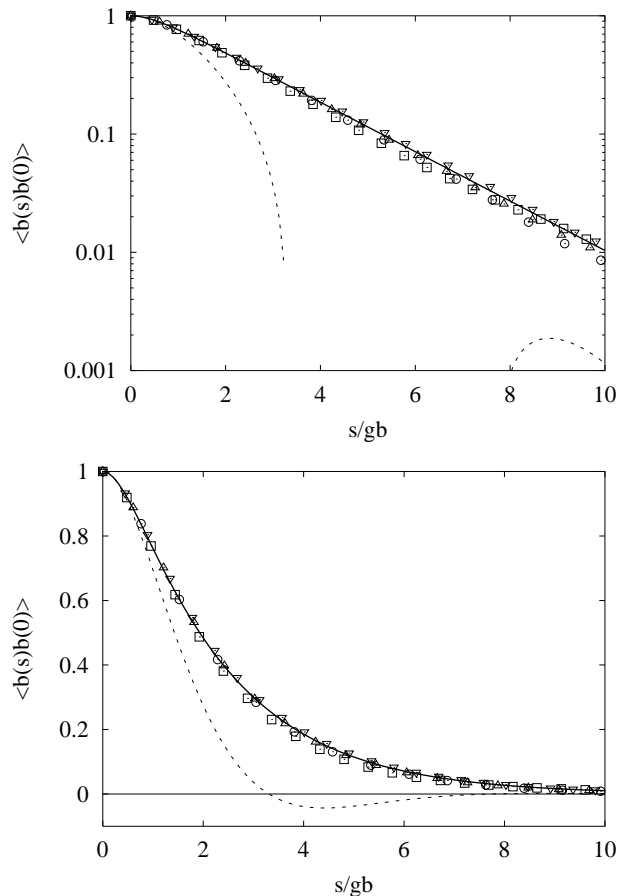


FIG. 5: (a) Autocorrelation function of the bond-directors with $k = 50$ (squares), $k = 100$ (circles), $k = 200$ (upward triangles), $k = 500$ (downward triangles) and $\alpha = \pi/3$. The data show the predicted functional (solid line) form for $\langle \mathbf{b}(0) \cdot \mathbf{b}(s) \rangle$ of Eq. (34). In order to check the scaling argument of Eq. (34) we determined the correct prefactor $g_{fit} = 0.56 \pm 0.05$ of g with the help of the numerical data of $\langle \theta_i \theta_j \rangle$ (see Fig. 3) and put it in Eq. (34). The agreement is excellent. The dashed line which oscillates is the predicted functional form of Liverpool *et al* [1, 2].

(b) Comparison of our simulation data with the analytical result of Liverpool *et al* (dashed line). The predicted oscillation and resultant pitch is not recovered. But we find the same scaling behavior of the helical persistence length with $l_b = gb \sim l_p^{1/3} a^{2/3}$. It is also striking that the predicted functional form of Liverpool *et al* is in very good agreement with our numerical data within one helical persistence length l_b .

with

$$\langle Tw(0, s)^2 \rangle = \frac{1}{3\pi^2} \left(\frac{s}{gb} - 2 \left(1 - \exp\left(-\frac{s}{2gb}\right) \right) \right) \quad (35)$$

and $gb = g_{fit}^{1/3} l_p^{1/3} a^{2/3} / 3^{1/3}$, where $g_{fit} = 0.56 \pm 0.05$ is the fitted prefactor for the scaling function g . a represents the strand separation of the ribbon which is given by $a = |\mathbf{b}_i| = \frac{1}{2} b \tan(\alpha)$. Hence we observe two length scales

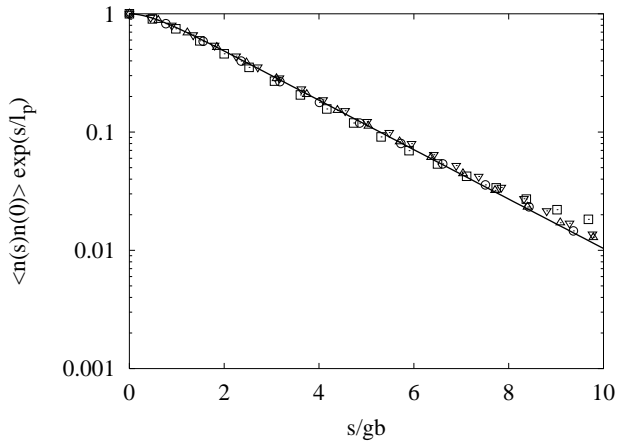


FIG. 6: Autocorrelation function of the normal vectors with $k = 50$ (squares), $k = 100$ (circles), $k = 200$ (upward triangles), $k = 500$ (downward triangles) and $\alpha = \pi/3$. We divided out of the normal vector correlation function (solid line) the tangent correlation function $\langle \mathbf{t}(0) \cdot \mathbf{t}(s) \rangle$ (see Eq. (36)) so that one should regain the same exponential decay as for $\langle \mathbf{b}(0) \cdot \mathbf{b}(s) \rangle$ which is in agreement with the numerical data.

influencing the local twist structure of the ribbon: on the one hand the single strand persistence length l_p and on the other hand the strand separation a . The predicted scaling behavior of $\langle \mathbf{b}(0) \cdot \mathbf{b}(s) \rangle$ can be observed in the simulation data as it is shown in Fig (5). Note that $\langle \mathbf{b}(0) \cdot \mathbf{b}(s) \rangle$ as well as all other calculated observables within this model is independent of the geometry of the triangles in contrast to the previous model where α was a fixed parameter.

Eq. (30) can be evaluated in the same manner resulting in

$$\begin{aligned} \langle \mathbf{n}(0) \cdot \mathbf{n}(s) \rangle &= \langle \mathbf{t}(0) \cdot \mathbf{t}(s) \rangle \langle \mathbf{b}(0) \cdot \mathbf{b}(s) \rangle \\ &= \exp\left(-\frac{s}{l_p} - 2\pi^2 \langle Tw(0, s)^2 \rangle\right). \end{aligned} \quad (36)$$

Eq.(34) shows that the autocorrelation function of the normal vectors is the product of $\langle \mathbf{t}(0) \cdot \mathbf{t}(s) \rangle$ and $\langle \mathbf{b}(0) \cdot \mathbf{b}(s) \rangle$. For very stiff chains, the tangent correlation function gives just small corrections to the normal vector correlation function. Therefore one can interpret Eq.(34) as the rigid rod limit of Eq.(36).

Other important structural properties of the ribbon can be extracted out of the crosscorrelation functions. $\langle \mathbf{n}(0) \cdot \mathbf{t}(s) \rangle$ and $\langle \mathbf{n}(0) \cdot \mathbf{b}(s) \rangle$ describe the mean curvature and mean twist respectively and vanish in both models for symmetry reasons. For $\langle \mathbf{b}(0) \cdot \mathbf{t}(s) \rangle$ we empirically observe the following relationship:

$$\langle \mathbf{b}(0) \cdot \mathbf{t}(s) \rangle = (2\pi)^2 a \frac{d}{ds} \langle Tw(0, s)^2 \rangle e^{-(2\pi)^2 \langle Tw(0, s)^2 \rangle}. \quad (37)$$

Eq. (37) can be understood qualitatively in the following way. Due to the anisotropic rigidity of the ribbon the

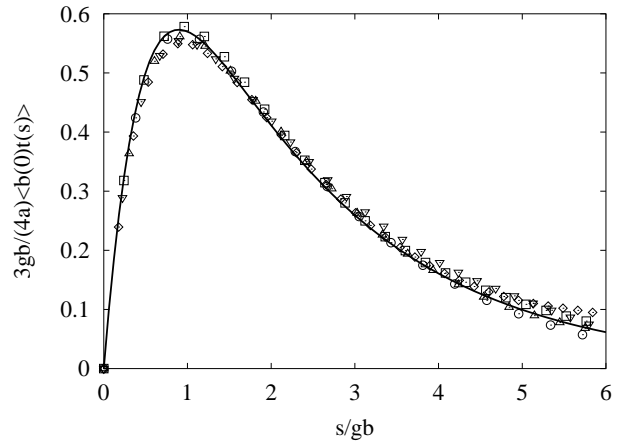


FIG. 7: Crosscorrelation function of the bond-directors and the tangent vectors with $k = 50$ (squares), $k = 100$ (circles), $k = 200$ (upward triangles), $k = 500$ (downward triangles), $k = 1000$ (diamonds) and $\alpha = \pi/3$. The data validate the predicted functional form (solid line) for $\langle \mathbf{b}(0) \cdot \mathbf{t}(s) \rangle$ of Eq. (37).

scalar product $\mathbf{b}(0) \cdot \mathbf{t}(s)$ is only non-zero if the chain is bent and twisted simultaneously. In case the ribbon is either solely bent or solely twisted the bond-directors are always perpendicular to the tangent vectors and the scalar product $\mathbf{b}(0) \cdot \mathbf{t}(s)$ vanishes for all s . The rate of mean twist of one helical persistence length $l_b = gb$ which defines the size of the locally existing helical structures can be calculated with Eq. 35 yielding $\sqrt{\langle Tw(0, bg)^2 \rangle} \approx \pm \frac{1}{16}$. This corresponds to a typical twist angle of $\Psi = \frac{\pi}{8}$ using $Tw = 2\pi\Psi$. Within l_b the twist rate is determined by the derivative of the mean squared twist $\frac{d}{ds} \langle Tw(0, s)^2 \rangle$ which gives rise to the increasing correlation function $\langle \mathbf{b}(0) \cdot \mathbf{t}(s) \rangle$ up to the maximum value at $l_b = gb$. For larger internal distances of the chain the rate of mean twist is a random sequence of $\pm \frac{1}{16}$ so that the crosscorrelation function has to vanish and therefore decreases exponentially with $\exp(-2\pi^2 \langle Tw(0, s)^2 \rangle)$. Fig. (7) compares Eq. (37) with our numerical data. The agreement is excellent.

VIII. BEHAVIOR UNDER COMPRESSION: EULER BUCKLING VS. KINKS

As discussed in section III the edge stiffness model includes local twist correlations at least on small length scales as a consequence of the correlation of the folding angles $\{\theta_i\}$. In order to understand and to quantify the effects arising from the local twist we measured the probability distribution functions of the folding angles, of the twist, and of the end-to-end-distance for different rigidities and compared the latter with the usual wormlike chain model to see which differences occur.

If there is a preference for kinking one can enforce this property by applying an additional constant force

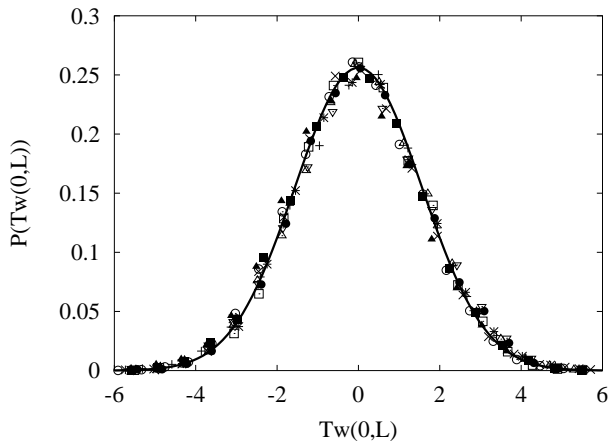


FIG. 8: Comparison of the probability distribution functions of the total twist of the ribbon for both models with $f = f = \{0, 0.01, 0.02, \dots, 0.09\}$ and $l_p = L = 400$ with the scaling analysis for $f = 0$. One recovers the same Gaussian shape for all values of f .

$\mathbf{F}_{buck} = f\mathbf{R}_E/R_E$ which compresses the ribbon. In addition the change in the end-to-end distance R_E caused by the buckling force should affect the twist distribution function $P(Tw)$ if R_E and Tw are coupled.

For small forces we calculate the change of twist under the influence of the external force $F_{buck} = f$ within the framework of linear response theory:

$$\begin{aligned} \langle \Delta Tw(0, L)^2 \rangle &= \langle Tw(0, L)^2 \rangle - \langle Tw(0, L)^2 \rangle_{f=0} \\ &= -\beta f (\langle R_E Tw(0, L)^2 \rangle_{f=0} - \langle R_E \rangle_{f=0} \langle Tw(0, L)^2 \rangle_{f=0}) \end{aligned} \quad (38)$$

with $\beta = 1/k_B T$. This predicts a change of the mean squared twist of the chain if a twist-stretch coupling determined by $\langle R_E Tw(0, L)^2 \rangle_{f=0}$ exists. Note that $\langle R_E Tw(0, L) \rangle_{f=0}$ vanishes due to symmetry reasons. The evaluation of our numerical data yields that $\langle R_E Tw(0, L)^2 \rangle$ is uncorrelated, too. To quantify if higher order terms in f contribute to a change of $\langle Tw(0, L)^2 \rangle$ we carried out several simulation runs with varying force strengths $f = \{0, 0.01, 0.02, \dots, 0.09\}$ corresponding to $\frac{R_E(f)}{R_E(0)} = \{1, 0.95, 0.87, 0.71, 0.51, 0.36, 0.26, 0.21, 0.17, 0.15\}$.

Fig. 8 shows the same Gaussian shape for all measured probability distribution functions of the total twist of the ribbon $P(Tw(0, L), f)$. This implicates that there is no twist-stretch coupling inherent in the system. The same is valid for the distribution function of the folding angles.

Moreover we measured the probability distribution function $P(R_E, f)$ of the end-to-end distance R_E for all applied forces f . Using the multiple histogram method developed by Ferrenberg and Swendsen [31] one can then recombine all measured histograms with a reweighting procedure to a single probability distribution function $P(R_E)$ with overall very good statistics. Fig. 9 shows

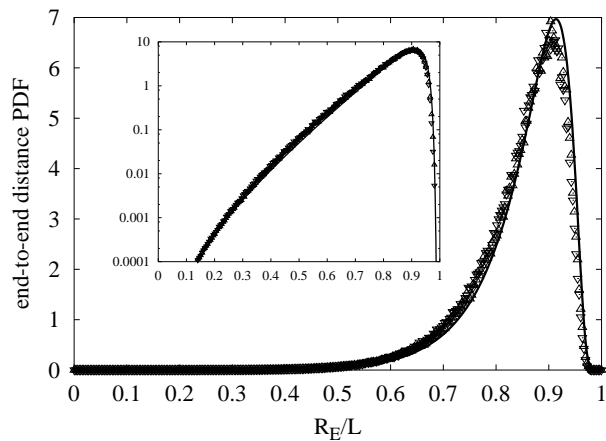


FIG. 9: Probability distribution functions of the end-to-end distance of the edge stiffness model for different discretizations ($N = 800$ upward triangles, $N = 600$ downward triangles) with $\alpha = \frac{\pi}{4}$ and $l_p = L = 400$ calculated with the help of the multiple histogram method [31] and the usual wormlike chain model (solid line). The PDF of the wormlike chain model is calculated with the derived analytical expression of Wilhelm and Frey [32].

$P(R_E)$ for \mathcal{H}_{tt} and the wormlike chain model. Quite contrary to a shift to noticeably shorter end-to-end distances R_E as one would expect for the above described phenomena of kinks one just recovers the usual wormlike chain behavior. This indicates that the ribbon just bends under the external force in contradiction to a kink-rod structure. Another quantity which is sensitive to the presence of kinks is a three-point correlation function of the end-to-end distance R_E and the twist to the left $Tw(0, \frac{L}{2})$, and to the right $Tw(\frac{L}{2}, L)$ of the center of the chain. Due to the buckling force the center of the chain is labeled which means that a kink is detected if the end-to-end distances with $Tw(0, \frac{L}{2})Tw(\frac{L}{2}, L) < 0$ (unlike twists meeting at the center) are smaller than the end-to-end distances with $Tw(0, \frac{L}{2})Tw(\frac{L}{2}, L) > 0$ (like twists meeting at the center). Fig. 10 shows the mean end-to-end distance depending on the value of $Tw(0, \frac{L}{2})Tw(\frac{L}{2}, L)$ for $l_p = 200$, $L = 400$, and $f = 0$, $f = 0.03$, $f = 0.06$. We do not find an asymmetry between like and unlike twists meeting at the center as it would support the prediction of kinks made by Liverpool *et al* [1, 2].

IX. SUMMARY

We have reinvestigated the mechanical properties of the model introduced by Liverpool *et al* [1, 2] of a double-stranded semiflexible polymer and rationalized the results of our MC simulations with the help of a simple scaling argument. We recover the predicted simple exponential decay of the tangent-tangent correlation function with the single strand persistence length l_p and that

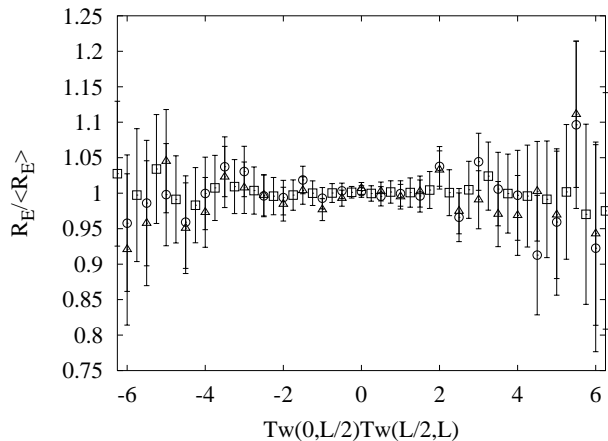


FIG. 10: End-to-end distance R_E as a function of the product of the twist left and right of the center of the chain $Tw(0, \frac{L}{2})Tw(\frac{L}{2}, L)$, which is a measure for unlike (negative sign) and like (positive sign) twists meeting at the center, and as a function of the applied buckling force with $f = 0$ (squares), 0.03 (circles), 0.06 (triangles) and $l_p = 0.5L = 200$. R_E refers to the average of one interval of $Tw(0, \frac{L}{2})Tw(\frac{L}{2}, L)$ and $\langle R_E \rangle$ refers to the mean value of all sampled end-to-end distances. One does not find an asymmetry between end-to-end distances for like and unlike twists meeting at the center. The larger fluctuations for larger values of $Tw(0, \frac{L}{2})Tw(\frac{L}{2}, L)$ are the result of a poorer sampling rate.

$\mathbf{t}(0) \cdot \mathbf{t}(s)$ is independent of the separation a of the two strands, which is in addition to l_p the other relevant length scale in the problem. Also in agreement with Ref. [1, 2] we find that the helical persistence length l_b and the helical pitch P scale with $l_p^{1/3} a^{2/3}$. Qualitatively, one would expect to see oscillations in the bond-director correlation function, if $P \leq l_b$. This can be understood by calculating the rate of mean twist within $l_b = gb$, i.e. $\sqrt{\langle Tw(0, gb)^2 \rangle}$. If the mean twist rate exceeds π an oscil-

latory behavior has to be observed. But our calculation gives a twist rate within $l_b = gb$ of approximately $\pm 1/16$. For larger distances of the chain the rate of mean twist is just given by a random sequence of $\pm 1/16$ and thus cannot account for an oscillatory behavior of $\langle \mathbf{b}(0) \cdot \mathbf{b}(s) \rangle$. Liverpool *et al* predict $P = l_b$, while our analysis indicates $P = 16l_b$ as it is demonstrated in Fig. 5 (b). The authors claimed support from their own simulations, but failed to provide a quantitative comparison between their numerical and analytical results. In fact the presented oscillations seem to be ordinary fluctuations within the statistical errors. But as can be seen in Fig. 5 (b) the predicted functional form for the bond-director autocorrelation function is in very good agreement with our numerical data as well as with our scaling results within one helical persistence length $l_b = gb$.

Moreover our simulation results with applied constant buckling forces do not provide any evidence of the predicted tendency of kinking or the claimed twist-stretch coupling. Thus contrary to the claim made in Ref. [1, 2] the local twist structure does not suffice to explain experimental observations such as the twist-stretch coupling [6, 33] and the kink-rod structures [34] of helical double-stranded molecules. These features require the inclusion of a spontaneous twist incorporated by an additional term in the Hamiltonian, e.g. $\mathcal{H}_{Tw} = k_{Tw} \sum_i \left(\sum_{j=i}^{i+1} \mathbf{n}_j \cdot \mathbf{b}_{j+1} - \theta_{sp,i} \right)^2$, [15, 16, 17, 18, 35, 36, 37, 38].

X. ACKNOWLEDGMENTS

The authors would like to thank B. Dünweg and H.J. Limbach, T.B. Liverpool, K. Kremer and H. Schiessel for numerous helpful discussions. Financial support from the DFG within the Emmy-Noether Programm is gratefully acknowledged.

-
- [1] T. B. Liverpool, R. Golestanian, and K. Kremer, *Phys. Rev. Lett.* **80**, 405 (1998).
[2] R. Golestanian and T. B. Liverpool, *Phys. Rev. E* **62**, 5488 (2000).
[3] T. T. Perkins, D. E. Smith, R. G. Larson, and S. Chu, *Science* **268**, 83 (1995).
[4] T. T. Perkins, D. E. Smith, and S. Chu, *Science* **276**, 2016 (1997).
[5] C. Bustamante, J. F. Marko, E. Siggia, and S. Smith, *Science* **265**, 1599 (1995).
[6] T. R. Strick, J.-F. Allemand, D. Bensimon, A. Bensimon, and V. Croquette, *Science* **271**, 1835 (1996).
[7] T. R. Strick, V. Croquette, and D. Bensimon, *Proc. Natl. Acad. Sci. USA* **95**, 10579 (1998).
[8] P. Cluzel *et al.*, *Science* **264**, 792 (1996).
[9] H. Yamakawa, *Helical Wormlike Chains in Polymer Solutions*, Springer, Berlin, 1997.
[10] J. F. Marko and E. D. Siggia, *Macromolecules* **28**, 8759 (1995).
[11] J. F. Marko and E. D. Siggia, *Macromolecules* **27**, 981 (1994).
[12] J. F. Marko and E. D. Siggia, *Phys. Rev. E* **52**, 2912 (1995).
[13] J. F. Marko and E. D. Siggia, *Science* **265**, 506 (1995).
[14] J. D. Moroz and P. Nelson, *Proc. Natl. Acad. Sci. USA* **94**, 14418 (1997).
[15] R. D. Kamien, T. C. Lubensky, P. Nelson, and C. S. O'Hern, *Europhys. Lett.* **38**, 237 (1997).
[16] S. Panyukov and Y. Rabin, *cond-mat/0105116* (2001).
[17] S. Panyukov and Y. Rabin, *Phys. Rev. E* **62**, 7135 (2000).
[18] S. Panyukov and Y. Rabin, *Phys. Rev. Lett.* **85**, 2404 (2000).

- [19] S. Kehrbaum and J. H. Maddocks, Philosophical Transactions Royal Society of London **355**, 2117 (1997).
- [20] R. S. Manning, J. H. Maddocks, and J. D. Kahn, J. Chem. Phys. **105**, 5626 (1996).
- [21] M. D. Frank-Kamenetskii, in *Numerical Data and Functional Relationships in Science and Technology*, edited by O. Madelung, VII/1c, Springer, Berlin, 1990.
- [22] R. Everaers, R. Bundschuh, and K. Kremer, Europhys. Lett. **29**, 263 (1995).
- [23] A. C. Maggs, J. Chem. Phys. **114**, 5888 (2001).
- [24] I. A. Nyrkova, A. N. Semenov, J.-F. Joanny, and A. R. Khokhlov, Journal de Physique II **6**, 1411 (1996).
- [25] Z. Zhou and P.-Y. Lai, Chem. Phys. Lett. **346**, 449 (2001).
- [26] D. M. Kroll and G. Gompper, Phys. Rev. A **46**, 3119 (1992).
- [27] N. Metropolis, A. W. Rosenbluth, M. N. Rosenbluth, A. N. Teller, and E. Teller, J. Chem. Phys. **21**, 1087 (1953).
- [28] D. P. Landau and K. Binder, *Monte Carlo Simulations in Statistical Physics*, Cambridge University Press, 2000.
- [29] H. Schiessel, W. M. Gelbart, and R. Bruinsma, Biophys. J. **80**, 1940 (2001).
- [30] M. Doi and S. Edwards, *The Theory of Polymer Dynamics*, Oxford University Press, 1986.
- [31] A. M. Ferrenberg and R. H. Swendsen, Phys. Rev. Lett. **63**, 1195 (1988).
- [32] J. Wilhelm and E. Frey, Phys. Rev. Lett. **77**, 2581 (1996).
- [33] T. R. Strick, J.-F. Allemand, D. Bensimon, and V. Croquette, Biophys. J. **74**, 2016 (1998).
- [34] J. Käs, H. Strey, M. Bärmann, and E. Sackmann, Europhys. Lett. **21**, 865 (1993).
- [35] J. F. Marko, Europhys. Lett. **38**, 183 (1997).
- [36] Z. Yang, Z. Haijun, and O.-Y. Zhong-can, Biophys. J. **78**, 1979 (2000).
- [37] Z. Haijun, Z. Yang, and O.-Y. Zhong-can, Phys. Rev. E **62**, 1045 (2000).
- [38] Z. Haijun, Z. Yang, and O.-Y. Zhong-can, Phys. Rev. Lett. **82**, 4560 (1999).